# Supplemental Information

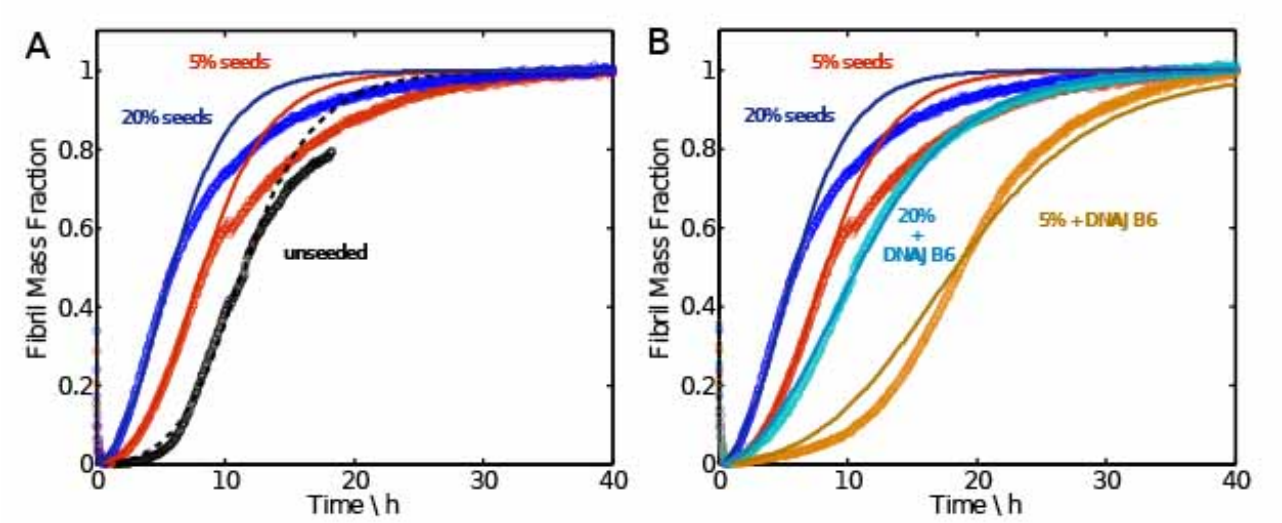


**Figure S 1: Kinetic analysis of seeded aggregation reactions of the polyQ peptide in the absence and presence of DNAJB6. (A)** the global fitting of reaction profiles initiated with different amounts of seeds confirms the presence of secondary nucleation events in the aggregation process of the 6 kDa polyQ peptide containing 45 glutamine residues; **(B)** in the presence of DNAJB6 at a molar ratio of 1:0.01, the apparent secondary nucleation rate is 25% of the value evaluated in the absence of the chaperone, indicating the capacity of DNAJB6 to interfere with secondary nucleation pathways when the chaperone is not sequestered by primary nuclei, as observed under unseeded conditions. The concentration of DNAJB6 is 10 µM in all cases. Data are taken from Månsson et al., Cell Stress Chaperones *19*, 227–239.

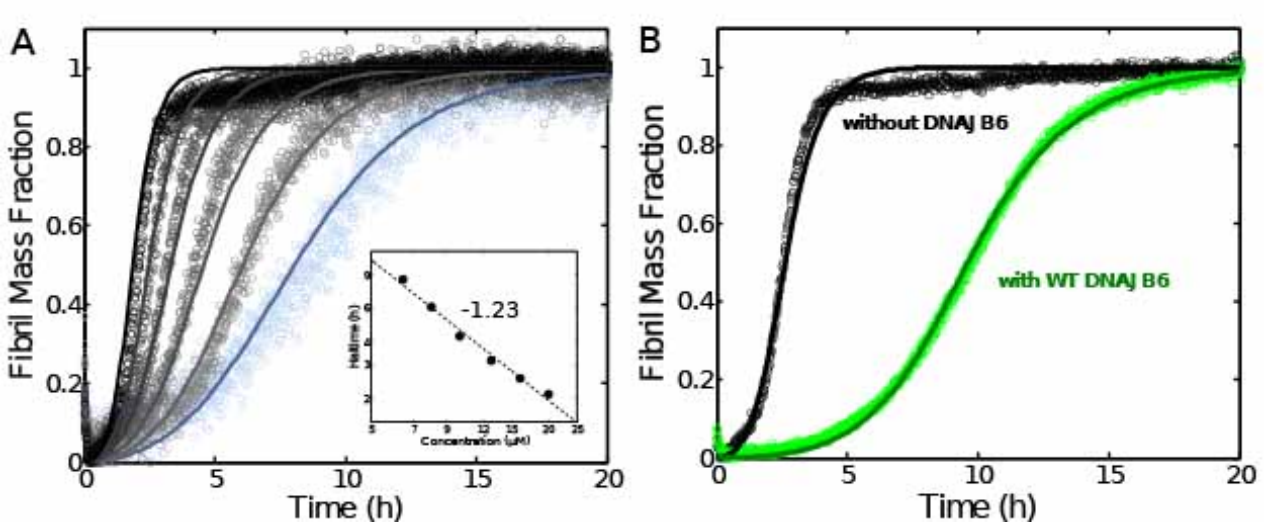


**Figure S2: Kinetic analysis of aggregation reactions of Htt-Exon 1 in the absence and presence of DNAJB6. (A)** Kinetic profiles of the aggregation of the 14 kDa Htt-Exon 1 containing 45 glutamine residues at concentrations of 6.4, 8, 10, 12.8, 16 and 20 µM monitored by ThT fluorescence. Continuous lines represent global fitting of the integrated rate laws to the data according to the equations in Supplementary Material. The inset shows the scaling of the half-time with peptide concentration, the value of which indicate the dominance of a secondary nucleation mechanism; **(B)** Kinetic profiles of the aggregation of 15 µM HttEx1Q45 peptide in the absence (black) and presence of DNAJB6 WT (green) at a molar ratio of 1:0.1. Continuous lines represent fits of integrated rate laws to the data. In the presence of the chaperone $k_n k_+/k_n k_+^* = 0.04$ and $k_2 k_+/k_2 k_+^* = 0.11$, where asterisk refers to conditions in the absence of DNAJB6. Data are taken from Månsson et al., Cell Stress Chaperones *19*, 227–239.

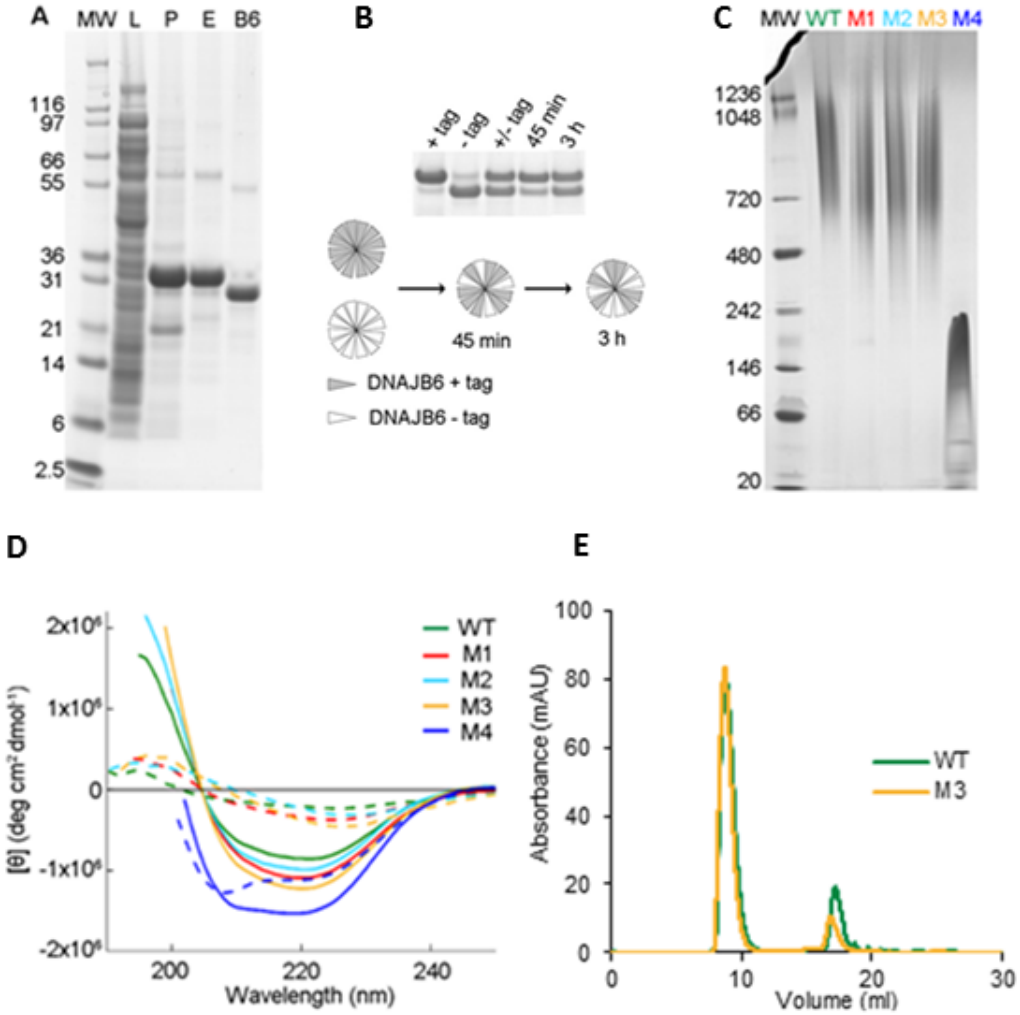


**Figure S3: Purification of the DNAJB6 protein and assessment of the structural integrity of mutational variants of DNAJB6. (A)** DNAJB6 was recombinantly expressed with a cleavable His-tag; various fractions from the purification procedure analyzed by CBB-stained SDS-PAGE. Molecular weight reference (MW). From the lysate (L) the inclusion body pellet (P) was recovered and dissolved in urea, and the His-tagged DNAJB6 was bound onto a nickel column, washed and refolded and recovered in the eluate (E). After cleavage with TEV protease, DNAJB6 without the His-tag was obtained in the flow-through after a second loading to the nickel column (B6). **(B)** The DNAJB6 chaperone is oligomeric, as shown by non-denaturing electrophoresis in (C), with subunits exchanging between oligomers on a time-scale of hous, as suggested from the changed composition of the eluate when aliquots from a 1:1 mixture with and without tag are loaded and eluted from the nickel column after different time points. **(C)** Assessment of WT DNAJB6 and its mutational variants M1-M4 by CBB-stained non-denaturing PAGE showing that WT and the substitution mutational variants M1-M3 are oligomeric whereas the deletion mutational variant M4 is not. **(D)** Assessment of the structural integrity of DNAJB6 WT and its mutational variants M1-M4 by CD spectroscopy. The molar ellipticity was measured at 37°C (continuous lines) and 75°C (dashed lines) showing high similarity in secondary structure for DNAJB6 WT and the substitution mutational variants M1-M3. **(E)** Size exclusion chromatography (SEC) was performed with DNAJB6 WT and the substitution mutational variant M3 on a Superdex 200 Increase 10/300 GL column with peaks eluting at 9 and 17 ml corresponding to 670 and 29 kDa, respectively (by courtesy of Gudrun Rutsdottir and Christopher Söderberg at MAX-lab at Lund University).

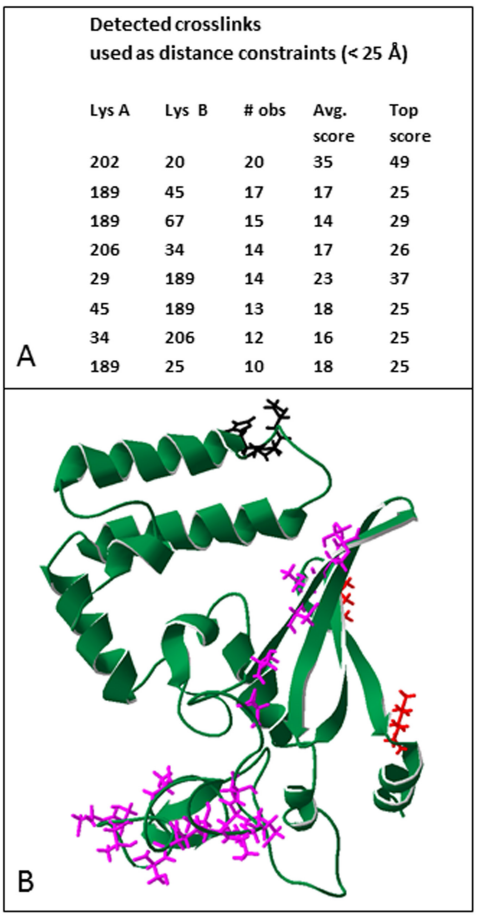

Detected crosslinks
used as distance constraints (< 25 Å)

| Lys A | Lys B | # obs | Avg. score | Top score |
|---|---|---|---|---|
| 202 | 20 | 20 | 35 | 49 |
| 189 | 45 | 17 | 17 | 25 |
| 189 | 67 | 15 | 14 | 29 |
| 206 | 34 | 14 | 17 | 26 |
| 29 | 189 | 14 | 23 | 37 |
| 45 | 189 | 13 | 18 | 25 |
| 34 | 206 | 12 | 16 | 25 |
| 189 | 25 | 10 | 18 | 25 |



**Figure S4: Structure model for the DNAJB6 monomer generated by combining structural modelling and crosslinking mass spectrometry. (A)** Intra-monomeric distance constraints between lysine residues in the N- and C-terminal domain of the DNAJB6 monomer obtained by lysine-specific crosslinking and mass spectrometry. The data files, used to detect the listed crosslinks with top score >25 and number of observations >10, as described in Materials and Methods, are publically available at ProteomeXchange (http://www.proteomexchange.org/). **(B)** The best-fit model of the DNAJB6 monomer in a ribbon representation, with highlighted amino acids: the serine and threonine residues (pink) in the conserved S/T-rich region (aa 155-195), which protrudes as a largely disordered domain between the well-ordered N- and C-terminal domains and presumably interacts with the polyQ-peptides, the conserved HPD motif (black, aa 31-33) that interacts with Hsp70 and the lysine residues K225 and K232 (red) that interact with a histone deacetylase.

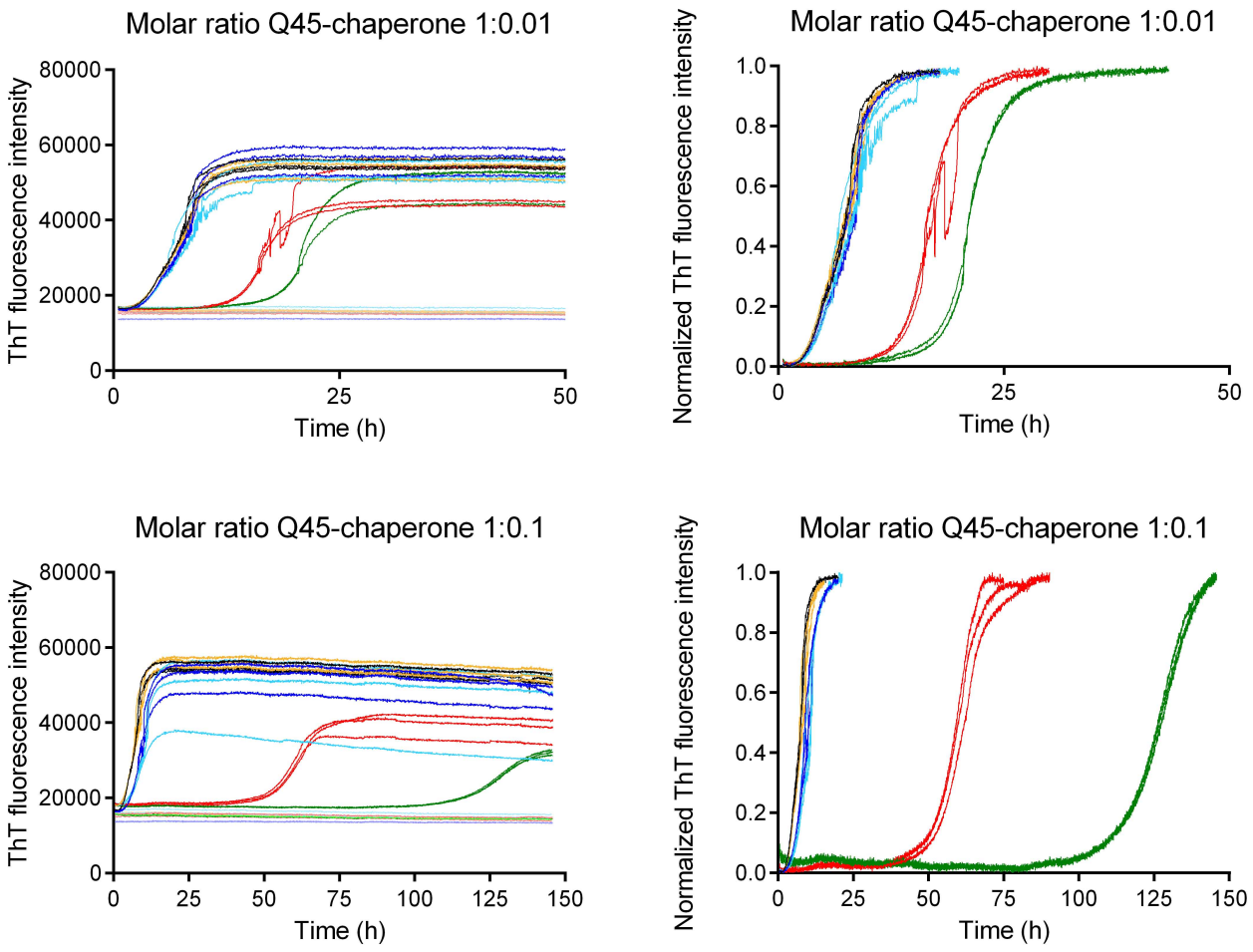


**Figure S5: Formation of polyQ fibrils monitored as ThT fluorescence in the absence and presence of DNAJB6.** Fibril formation was monitored by following the increase in ThT fluorescence with triplicate curves with the following color coding: polyQ without chaperone addition (black), WT DNAJB6 (green), and DNAJB6 mutants M1 (red), M2 (turquoise), M3 (orange), M4 (blue). Non-normalized curves (left), with control samples without polyQ peptides shown in faded colors and normalized curves (right), both at molar ratios of polyQ to DNAJB6 of 1:0.01 (upper) and 1:0.1 (lower).

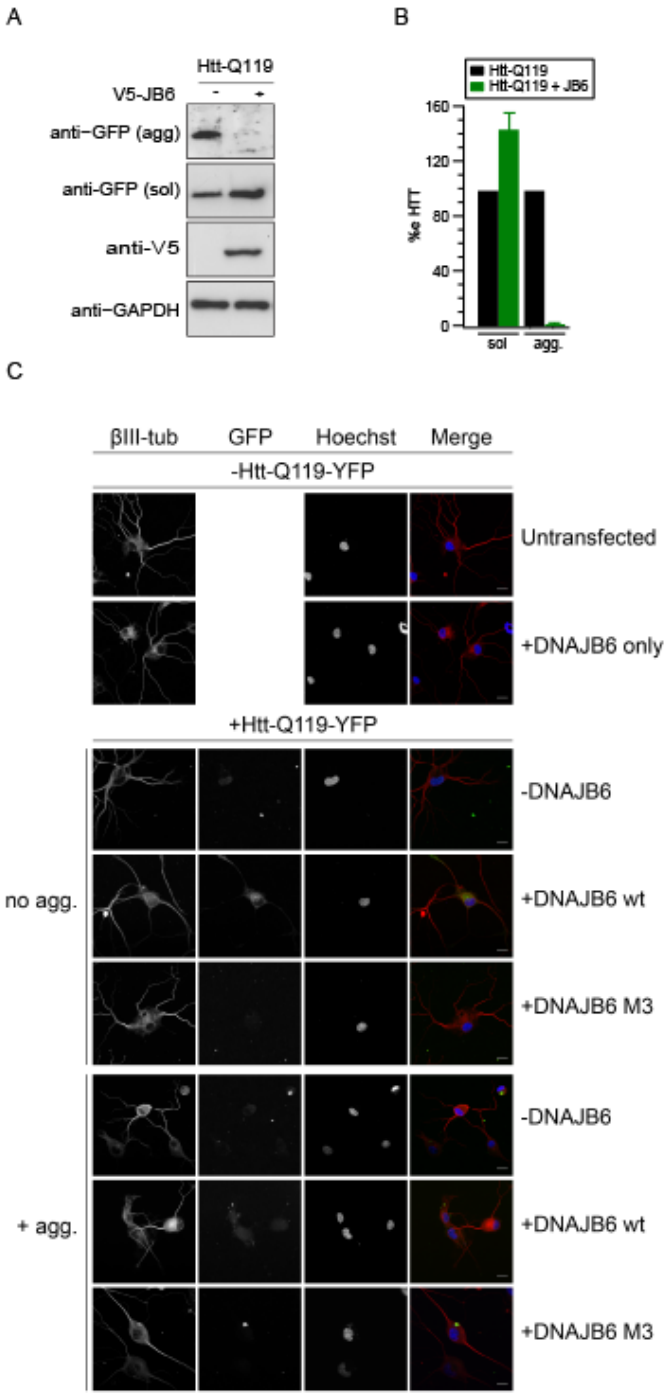


**Figure S6: PolyQ aggregation and neurite formation in differentiated NG108 cells transfected with Htt-Q119-GFP alone or with V5-DNAJB6 (JB6) or with the V5-DNAJB6 M3 (JB6 M3) mutational variant (see fig 1).** NG108 cells were differentiated for 48 h with NECA and IBMX prior to transfection. **(A)** High molecular weight aggregated (agg: stacking gel) and soluble (sol) forms of Htt-Q119-eYFP were assessed with anti-GFP antibodies and **(B)** quantified by densitometry (mean + SD of 2 experiments). **(C)** Representative confocal pictures of differentiated NG108 cells co-transfected with Htt-Q119-GFP alone or JB6 or a combination of Htt-Q119-GFP with JB6 or JB6 M3. Images of with cells with and without polyQ aggregates are depicted. Images are counterstained with β-III tubulin (red) to stain neuronal processes and with DAPI (blue) to stain nuclei.

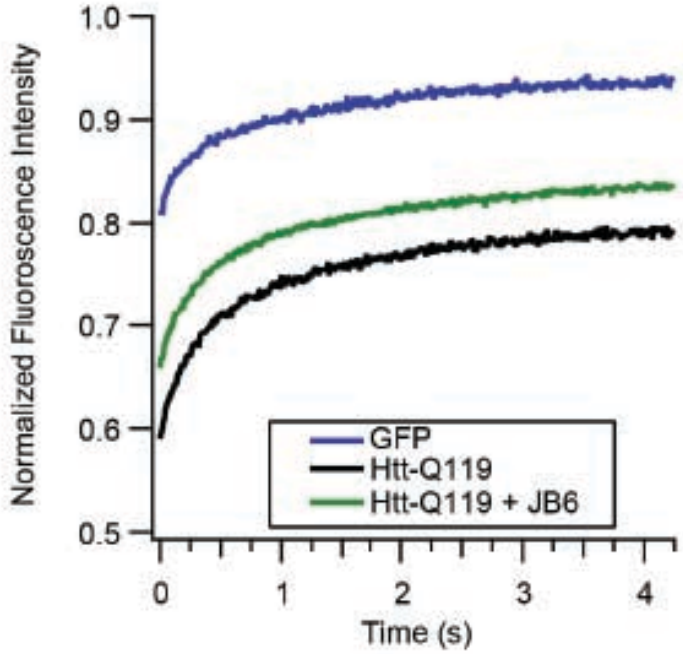


**Figure S7: DNAJB6 increases the fraction of mobile polyQ protein outside areas of visible aggregation in neuronal cells.** FRAP analysis for NG108 cells expressing Htt-Q119-eYFP alone or together with RFP-DNAJB6 or the V5-DNAJB6 H/Q mutant (that is unable to interact with Hsp70), analyzed 12 h post transfection and before the aggregates were visible.

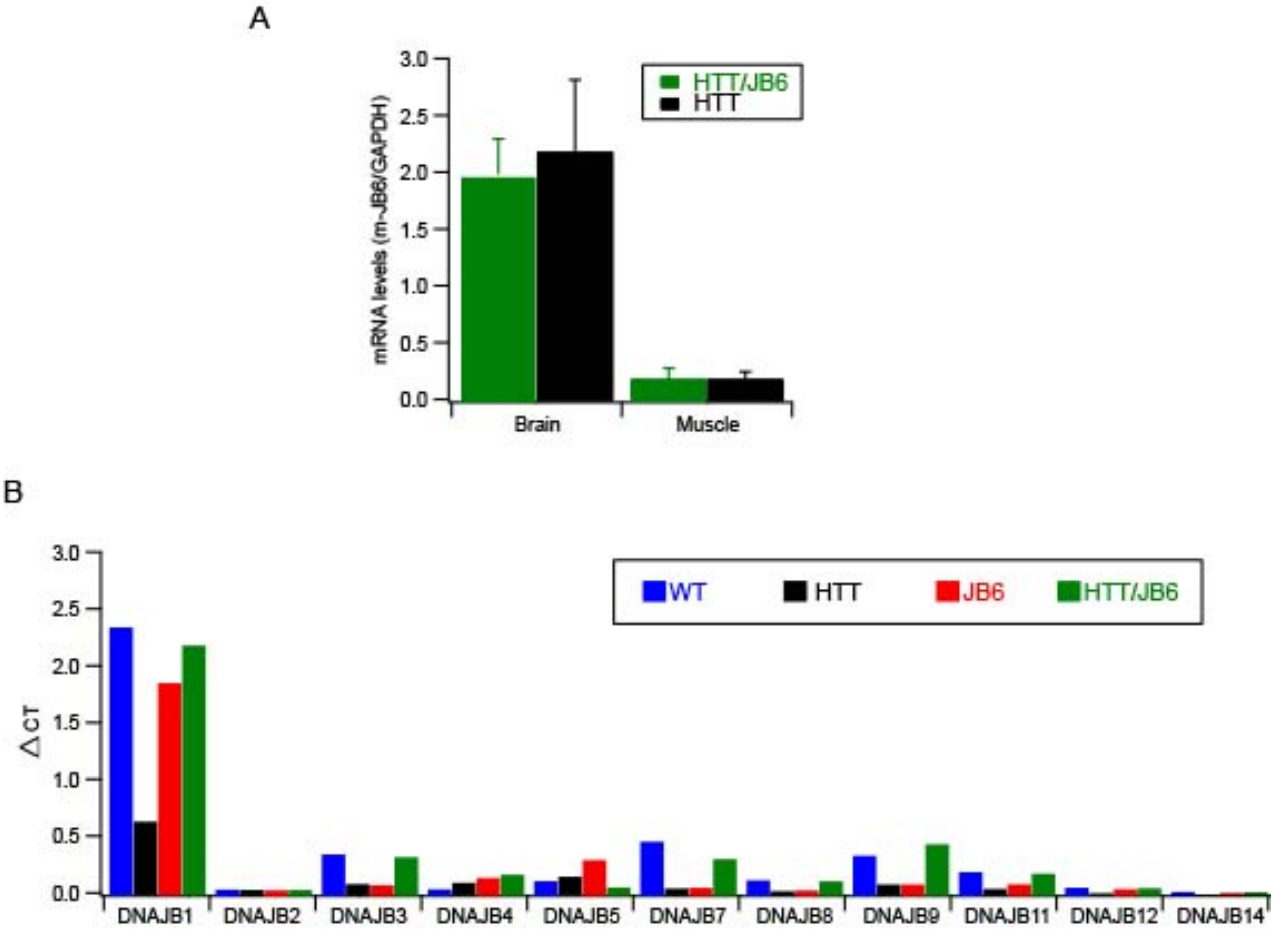


**Figure S8: Transcript levels of endogenous DNAJB6 and several other DNAJs from transgenic and WT mice. (A)** mRNA levels of endogenous DNAJB6 transcripts from brain and muscle lysates from both R6/2 mice (HTT: black) and R6/2 mice x DNAJB5 mice (HTT/JB6: green). The values were normalized with GAPDH levels in each sample. **(B)** qPCR data from control wildtype mice (WT: bleu), DNAJB6 transgenic mice (JB6: red), R6/2 mice (HTT: black) and R6/2 mice x DNAJB5 mice (HTT/JB6: green). Delta-CT values of the qPCR are given.

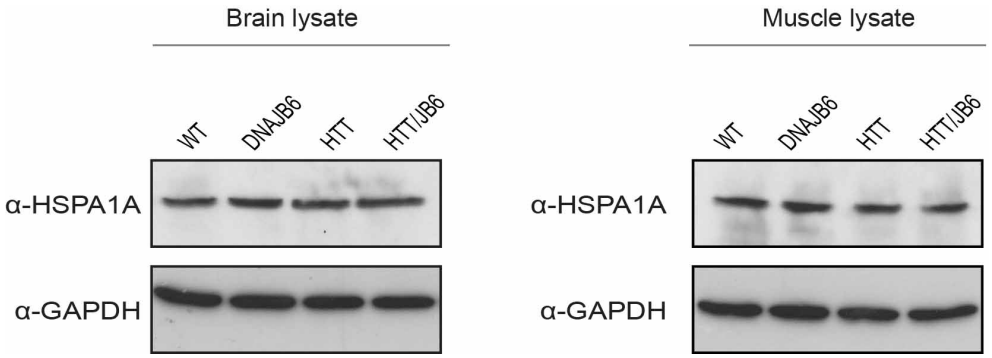


**Figure S9: HSPA1A levels remain unaltered in the transgenic DNAJB6 mouse as compared to WT animal.** Brain and muscle lysates from 12 week old animals were immune-blotted for Hsp70 levels using the anti-HSPA1A/Hsp70 (SPA-810: Stressgen,) antibody. GAPDH was used as loading control.

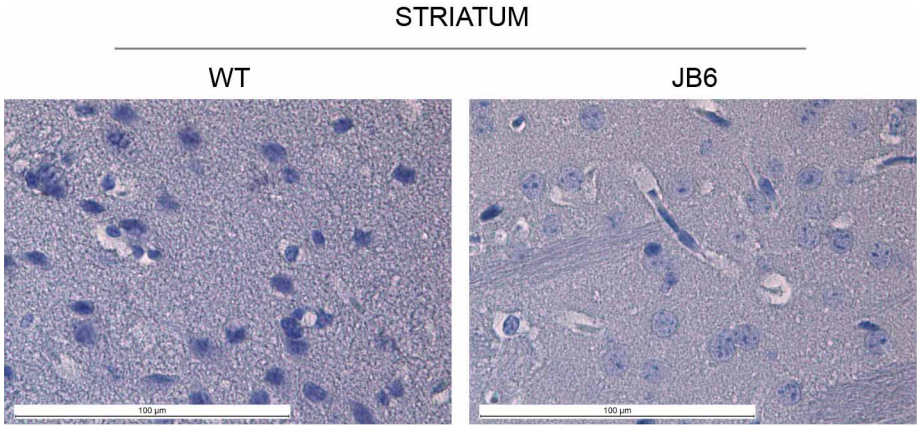


**Figure S10: DNAJB6 mice and WT control mice show no aggregates at 12 weeks of age.** Representative immunohistochemical pictures of striatum of WT and *TgDNAJB6* (*JB6*) control animals at 12 weeks of age. Hematoxylin was used to counterstain nuclei (blue stain) and EM48 to visualize HTT aggregates (brown staining). Scale: 100 µm. No aggregates (absence of brown staining) were visible in any of these groups.

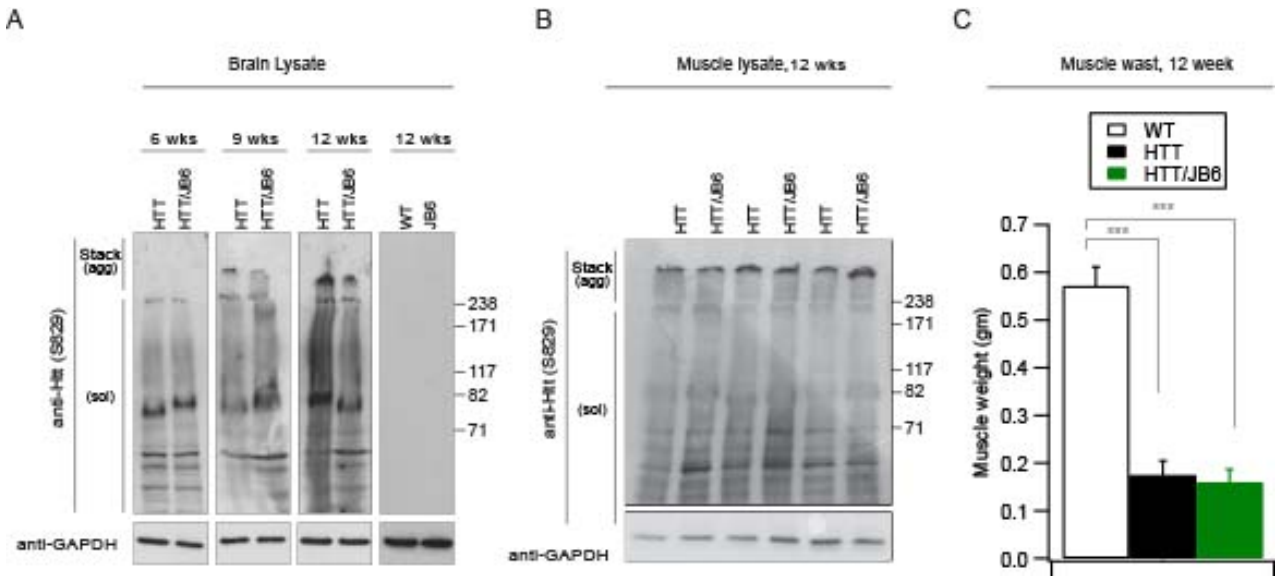


**Figure S11: polyQ aggregation in total brain (A) and muscle (B) lysates and muscles wasting (C) in animals from both HTT and HTT/JB6 group.**

Huntingtin aggregates (agg in stacking gels) and soluble material (sol) were detected using the S829 antibody in total brain (A: 6-12 weeks) or in skeletal muscle (B: 12 weeks) lysates and found to be reduced in brains of HTT/JB6 double transgenic mice compared to HTT mice at 9 and 12 weeks. However, In muscle lysates aggregation was found to be unaltered in double transgenic mice HTT/JB6 compared to HTT mice at all time points (data shown for week 12). (C) Muscle wasting (here shown at 12 weeks) due to expression of HTT was unaffected by co-expression of DNAJB6. The statistical significance was analysed using an independent t-test (*** P=0.0005, (± sem, n=8 for each group).

A

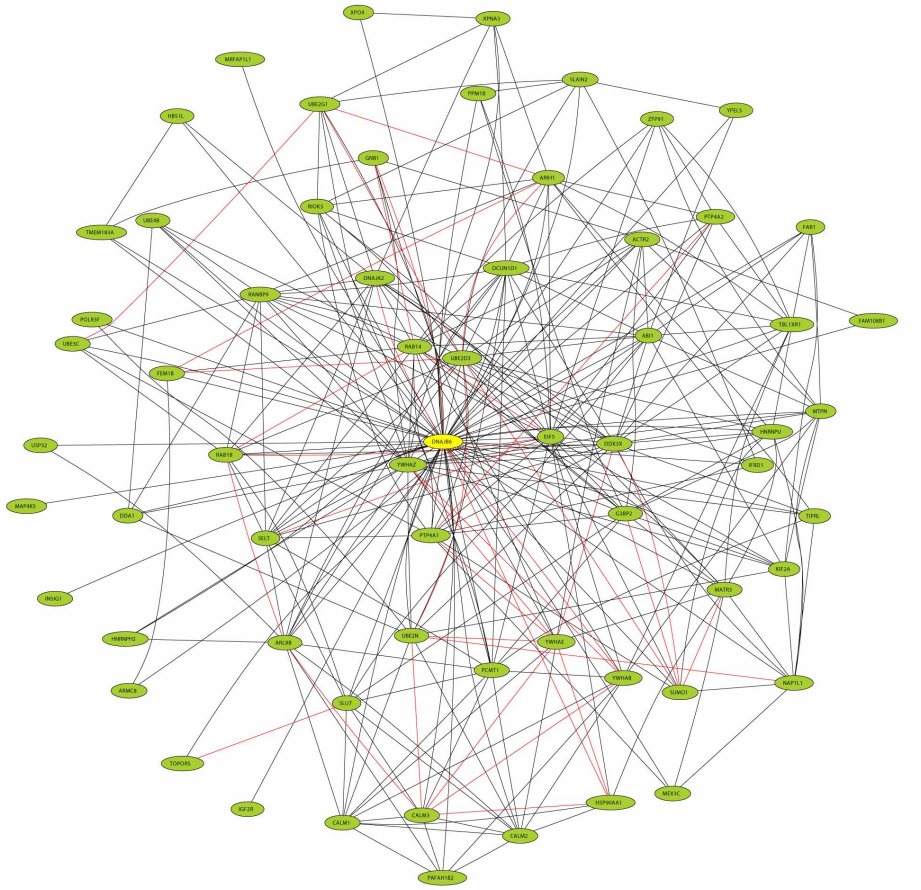

B

| Report for DNAJB6 (Gene ID 10049) | | | |
|---|---|---|---|
| GO ID | P-value | E-value | Description |
| 6511 | 4.46887e09 | 4.62081e-05 | ubiquitin-dependent protein catabolic process |
| 19941 | 4.56981e-09 | 4.72518e-05 | modification-dependent protein catabolic process |
| 51603 | 4.56981e-09 | 4.72518e-05 | proteolysis involved in cellular protein catabolic process |
| 43632 | 4.56981e-09 | 4.72518e-05 | modification-dependent macromolecule catabolic |
| 44257 | 4.77792e-09 | 4.94037e-05 | cellular protein catabolic process |
| 34962 | 4.77792e-09 | 4.94037e-05 | cellular biopolymer catabolic process |
| 30163 | 8.56545e-09 | 8.85668e-05 | protein catabolic process |
| 43285 | 5.52818e-08 | 0.000571614 | biopolymer catabolic process |
| 44265 | 1.48511e-07 | 0.0015356 | cellular macromolecule catabolic process |
| 19787 | 1.58303e-07 | 0.00163685 | small conjugating protein ligase activity |
| 9057 | 2.48054e-07 | 0.00256488 | macromolecule catabolic process |
| 16881 | 8.01449e-07 | 0.00828698 | acid-amino acid ligase activity |
| 4842 | 1.60919e-06 | 0.016639 | ubiquitin-protein ligase activity |
| 43687 | 2.09204e-06 | 0.0216317 | post-translational protein modification |
| 9056 | 3.14854e-06 | 0.0325559 | catabolic process |
| 6508 | 4.37728e-06 | 0.0452611 | proteolysis |
| 44248 | 4.47605e-06 | 0.0462824 | cellular catabolic process |
| 48770 | 6.19915e-06 | 0.0640992 | pigment granule |
| 42470 | 6.19915e-06 | 0.0640992 | melanosome |
| 16874 | 1.11458e-05 | 0.115248 | Ligase activity |
| 32446 | 1.21705e-05 | 0.125843 | protein modification by small protein conjugation |
| 3924 | 1.42068e-05 | 0.146898 | GTPase activity |
| 6464 | 3.26471e-05 | 0.337571 | protein modification process |
| 43412 | 5.24373e-05 | 0.542202 | biopolymer modification |

**Figure S12: DNAJB6 co-expression network and functional prediction.** Coexpression analysis of DNAJB6 obtained using the TS-CoExp browser (Piro et al., 2011) **(A)** Diagram of DNAJB6 co-expression network (black lines co-expression only; red lines co-expression + functional relation) **(B)** co-expression based prediction of possible functionalities of DNAJB6

**Table S1:**

**List of Primers used**

| **Primers** | **Sequence (5' – 3' )** |
|---|---|
| R6/2 fwd | CGC AGG CTA GGG CTG TCA ATC ATG CT |
| R6/2 rev | TCA TCA GCT TTT CCA GGG TCG CCA T |
| HDAC4 WT fwd | CTT GTT GAG AAC AAA CTC CTG CAG CT |
| HDAC4 WT rev | AGC CCT ACA CTA GTG TGT GTT ACA CA |
| DNAJB6 fwd (hDNAJB6) | GAC GAT GAC GAC AAG ATG GTG |
| DNAJB6 rev (hDNAJB6) | CCG TTT CTT AGC ATC CGA CAG |
| CRE fwd | GCG GTC TGG CAG TAA AAA CTA TC |
| CRE rev | ACG AAC CTG GTC GAA ATC AGT G |
| PCR CONTROL fwd | GGG ACC ACC TTC TTT TGG CTT C |
| PCR CONTROL rev | AAG ATG TGG AGA GTT CGG GGT AG |
| DNAJB6 fwd (mDNAJB6) | CTA CGA CAA ATA TGG CAA AGA AGG |
| DNAJB6 rev (mDNAJB6) | CGG AAT GTG AAG CCA AAC TC |
| NEO fwd | GCT CGA CGT TGT CAC TGA AG |
| NEO rev | CCA TTT TCC ACC ATG ATA TTC G |
| 40256 fwd (FAM labelled) | GAG TCC CTC AAG TCC TTC CAG CA |
| 40261 rev | GCC CAA ACT CAC GGT CGG T |